

Planar wallpaper group metamaterial for novel terahertz applications

Christopher M. Bingham¹, Hu Tao², Xianliang Liu¹, Richard D. Averitt³, Xin Zhang², and Willie J. Padilla¹

¹*Department of Physics, Boston College, 140 Commonwealth Ave., Chestnut Hill, Massachusetts 02467, USA.*

²*Boston University, Department of Manufacturing Engineering, 15 Saint Mary's Street, Brookline, Massachusetts 02446, USA.*

³*Department of Physics, Boston University, 590 Commonwealth Avenue, Boston, Massachusetts 02215, USA.*

binghach@bc.edu

Abstract: We present novel metamaterial structures based upon various planar wallpaper groups, in both hexagonal and square unit cells. An investigation of metamaterials consisting of one, two, and three unique sub-lattices with resonant frequencies in the terahertz (THz) was performed. We describe the theory, and perform simulations and experiments to characterize these multiple element metamaterials. A method for using these new structures as a means for bio / chemical hazard detection, as well as electromagnetic signature control is proposed.

© 2018 Optical Society of America

OCIS codes: (040.1880) Detection; (070.4790) Spectrum Analysis; (160.3918) Metamaterials; (300.6495) Spectroscopy, THz

References and links

1. V. G. Veselago, "The electrodynamics of substances with simultaneously negative values of ϵ and μ ," *Sov. Phys. Usp.* **10**, 509–614 (1968).
2. D. R. Smith, W. J. Padilla, D. C. Vier, S. C. Nemat-Nasser, and S. Schultz, "Composite Medium with Simultaneously Negative Permeability and Permittivity," *Phys. Rev. Lett.* **84**, 4184–4187 (2000).
3. R. A. Shelby, D. R. Smith, and S. Schultz, "Experimental Verification of a Negative Index of Refraction," *Science* **292**, 77–79 (2001).
4. J. B. Pendry, "Negative refraction makes a perfect lens," *Phys. Rev. Lett.* **85**, 3966 (2000).
5. A. Grbic and G. V. Eleftheriades, "Overcoming the Diffraction Limit with a Planar Left-Handed Transmission-Line Lens," *Phys. Rev. Lett.* **92**, 117403 (2004).
6. J. B. Pendry, D. Schurig, and D. R. Smith, "Controlling Electromagnetic Fields," *Science* **312**, 1780–1782 (2006).
7. D. Schurig, J. J. Mock, B. J. Justice, S. A. Cummer, J. B. Pendry, A. F. Starr, and D. R. Smith, "Metamaterial Electromagnetic Cloak at Microwave Frequencies," *Science* **314**, 977–979 (2006).
8. J. B. Pendry, A. J. Holden, D. J. Robbins, and W. J. Stewart, "Magnetism from conductors and enhanced nonlinear phenomena," *IEEE Trans. Microwave Theory Tech.* **47**, 2075–2084 (1999).
9. M. C. K. Siltshire, J. B. Pendry, I. R. Young, D. J. Larkman, D. J. Gilderdale, & J. V. Hajnal, "Microstructured magnetic materials for RF flux guides in magnetic resonance imaging," *Science* **291**, 849–851 (2001).
10. D. R. Smith, W. J. Padilla, D. C. Vier, S. C. Nemat-Nasser, S. Schultz, "Composite medium with simultaneously negative permeability and permittivity," *Phys. Rev. Lett.* **84**, 4184 (2000).
11. D. Schurig, J. J. Mock, and D. R. Smith, "Electric-field-coupled resonators for negative permittivity metamaterials," *Appl. Phys. Lett.* **88**, 041109 (2006).
12. M. Gokkavas, K. Guven, I. Bulu, K. Aydin, R. S. Penciu, M. Kafesaki, C. M. Soukoulis, and E. Ozbay, "Experimental demonstration of a left-handed metamaterial operating at 100 GHz," *Phys. Rev. B* **73**, 193103 (2006).
13. T. J. Yen, W. J. Padilla, N. Fang, D. C. Vier, D. R. Smith, J. B. Pendry, D. N. Basov, and X. Zhang, "Terahertz Magnetic Response from Artificial Materials," *Science* **303**, 1494–1496 (2004).

14. S. Linden, C. Enkrich, M. Wegener, J. Zhou, T. Koschny, and C. M. Soukoulis, "Magnetic Response of Metamaterials at 100 Terahertz," *Science* **306**, 1351-1353 (2004).
15. S. Zhang, W. Fan, N. C. Panoiu, K. J. Malloy, R. M. Osgood, and S. R. J. Brueck, "Experimental Demonstration of Near-Infrared Negative-Index Metamaterials," *Phys. Rev. Lett.* **95**, 137404 (2005).
16. U. K. Chettiar, A. V. Kildishev, T. A. Klar, and V. M. Shalaev, "Negative index metamaterial combining magnetic resonators with metal films," *Opt. Exp.*, textbf14, 7872-77 (2006).
17. G. Dolling, M. Wegener, C. M. Soukoulis, and S. Linden, "Negative-index metamaterial at 780 nm wavelength," *Opt. Lett.* **32**, 53-55 (2007).
18. V. M. Shalaev, W. Cai, U. K. Chettiar, H.-K. Yuan, A. K. Sarychev, V. P. Drachev, and A. V. Kildishev, "Negative index of refraction in optical metamaterials," *Opt. Lett.* **30**, 3356 (2005)
19. D. Schattschneider, "The Plane Symmetry Groups: Their Recognition and Notation," *The American Mathematical Monthly*, Vol. **85**, No. **6**, pp. 439-450 (1978)
20. T. Driscoll, G. O. Andrew, D. N. Basov, S. Palit, T. Ren, J. Mock, S.-Y. Cho, N. M. Jokerst, and D. R. Smith, "Quantitative investigation of a terahertz artificial magnetic resonance using oblique angle spectroscopy," *Appl. Phys. Lett.* **90**, 092508 (2007).
21. [18] being an exception having a hexagonal lattice.
22. Y. Yuan, C. Bingham, T. Tyler, S. Palit, T. H. Hand, W. J. Padilla, D. R. Smith, N. M. Jokerst, and S. A. Cummer, "Dual-band planar electric metamaterial in the terahertz regime," *Opt. Express* **16**, 9746-9752 (2008).
23. W. J. Padilla, M. T. Aronsson, C. Highstrete, M. Lee, A. J. Taylor and R. D. Averitt, "Electrically resonant terahertz metamaterials: Theoretical and experimental investigations," *Phys. Rev. B* **75**, 041102R (2007).
24. HFSS, Ansoft Corporation, Copyright (2008).
25. W. J. Padilla, A. J. Taylor, C. Highstrete, M. Lee, and R. D. Averitt, "Dynamical Electric and Magnetic Metamaterial Response at Terahertz Frequencies," *Phys. Rev. Lett.* **96**, 107401 (2006).
26. H. Tao, N. I. Landy, C. M. Bingham, X. Zhan, R. D. Averitt, and W. J. Padilla, "A metamaterial absorber for the terahertz regime: design, fabrication and characterization," *Opt. Express* **16**, 7181-7188 (2008).
27. Brucherseifer, M., M. Nagel, P. H. Bolivar, H. Kurz, A. Bosserhoff, and R. Buttner, "Label-free probing of the binding state of DNA by time-domain terahertz sensing," *Appl. Phys. Lett.* **77**, 4049-4051 (2000).
28. A. Menikh, S. P. Mickan, H. Liu, R. MacColl, and X.-C. Zhang, "Label-free amplified bioaffinity detection using terahertz wave technology," *Biosens. Bioelectron.* **20**, 658662 (2004).
29. W. J. Padilla, A. J. Taylor, C. Highstrete, M. Lee, R. D. Averitt, "Dynamical electric and magnetic metamaterial response at terahertz frequencies," *Phys. Rev. Lett.* **96**, 107401 (2006).
30. H.-T. Chen, W. J. Padilla, J. M. O. Zide, A. C. Gossard, A. J. Taylor, R. D. Averitt, "Active terahertz metamaterial devices," *Nature* **444**, 597-600 (2006).
31. T. M. Korter, D. F. Plusquellic, "Continuous-wave terahertz spectroscopy of biotin: vibrational anharmonicity in the far-infrared," *Chem. Phys. Lett.* **385**, 45-51 (2004).
32. D. G. Allis, A. M. Fedor, T. M. Korter, J. E. Bjarnason, E. R. Brown "Assignment of the lowest-lying THz absorption signatures in biotin and lactose monohydrate by solid-state density functional theory," *Chem. Phys. Lett.* **440** 203-209 (2007).
33. Z. Jakšić, O. Jakšić, Z. Djurić and C. Kment, "A consideration of the use of metamaterials for sensing applications: field fluctuations and ultimate performance," *J. Opt. A: Pure Appl. Opt.* **9** S377-S384 (2007).
34. J. F. O'Hara, R. Singh, I. Brener, E. Smirnova, J. Han, A. J. Taylor, and W. Zhang, "Thin-film sensing with planar terahertz metamaterials: sensitivity and limitations," *Optics Express*, **16**, 1786-1795 (2008).
35. M. Osawa, "Surface Enhanced Infrared Absorption," *Topics Appl. Phys.* **81** 163-187 (2001), and references contained therein.
36. M. Tabor, "Chaos and Integrability in Nonlinear Dynamics: An Introduction," New York: Wiley, pp. 154-163 (1989).
37. B. V. Chirikov, "A Universal Instability of Many-Dimensional Oscillator Systems," *Phys. Rep.* **52** 264-379 (1979).
38. S. P. Mickan, A. Menikh, H. Liu, C. A. Mannella, R. MacColl, D. Abbott, J. Munch and X-C Zhang, "Label-free bioaffinity detection using terahertz technology," *Phys. Med. Biol.* **47** 3789-3795 (2002).
39. N. I. Landy, S. Sajuyigbe, J. J. Mock, D. R. Smith, and W. J. Padilla, "Perfect Metamaterial Absorber," *Phys. Rev. Lett.* **100**, 207402 (2008).

1. Introduction

Over the last several years the field of metamaterials has seen enormous and consistent growth. Initially this was due to the demonstration of negative refractive index (NRI), or "left-handed materials" as it was termed [1, 2, 3], as well as the prediction and verification of the "perfect lens" [4, 5]. This led to strong interest from scientists in many varied areas and spawned nu-

merous major research thrusts thus engaging a worldwide community. Metamaterials received another enormous boost recently when it was discovered that it is possible to construct a cloak - an advanced structure that makes an object “invisible” to interrogating light of a particular wavelength [6, 7]. Present excitement in metamaterials stems from their ability to access regimes of material response not possible with naturally occurring materials. They also serve as a platform to explore new physics in an otherwise mature science field - classical electricity and magnetism.









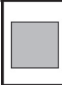
NRI and cloaking are certainly booming areas of scientific exploration and largely responsible for the immense growth of metamaterials. However, artificial materials represent a new paradigm for the construction of novel devices, and metamaterials are much broader than just the examples listed above. Arguably, the real power in metamaterials lies in the fact that it is possible to construct materials with an exact magnetic and electric response. For example, the so-called “split ring resonator” [8] has been the standard metamaterial utilized for magnetic response across much of the electromagnetic (EM) spectrum. With SRR type structures demonstrated at radio [9], microwave [10, 11], mm-Wave [12], THz [13], MIR [14], NIR [15, 16] to the optical [17, 18] the design has proven to be very versatile. The majority of prior metamaterials work has used simple variations of the split ring design and/or straight wire media.

Although the above listed successes of metamaterials evince their ability to access exotic EM responses and highlight their great technical potential, they still face several major obstacles which must be overcome before widespread usage in devices is possible. For example, researchers strive to construct metamaterials such that they may be described by bulk material parameters characterizing their frequency dependent effective electric $\epsilon(\omega)$ and effective magnetic $\mu(\omega)$ EM responses. As such, most designs are based on resonances in order that the physical dimensions of the unit cell (a) and the metamaterial itself (L) are smaller than the wavelength at resonance λ_0 , i.e. $L < a \ll \lambda_0$. This resonant behavior is, of course, what permits metamaterials to attain electromagnetic responses which deviates from unity - the free space values - thereby achieving the exotic behaviors noted above. However, a consequence of this strong frequency dispersion is that the novel responses that metamaterials achieve are often narrow band, typically $<5\%$. The combination of wire media and SRRs (along with other similar variants) has also yielded great triumphs, however these designs will still be limited by narrow band behavior and the metamaterial responses achievable through combination. An important step in the creation of artificial materials is to create designs that can mimic the many various types of symmetries that are observed in nature.

We present new metamaterial geometries which may be oriented in various different planar wallpaper groups that significantly extend the pallet of available structures beyond simple square lattices of wire and SRR arrays. Further, these new metamaterials may help to alleviate the narrow-band response of metamaterials by permitting multi-frequency response without significantly compromising “electromagnetic strength”. We detail the theory, simulation, fabrication, and measurement of several of these metamaterials at THz frequencies. Several potential applications of these new MMs are discussed including electromagnetic signature control and biodetection.

2. Theory

The analogy between metamaterials and real materials can be extended, beyond what has been shown before, by appealing to designs that nature has provided. For example, condensed matter describes materials consisting of different elements as a Bravais lattice with a basis. In a similar manner, we can form metamaterials that have more than one primitive cell, where each has a distinct metamaterial element, and distinct electromagnetic properties. These individual cells may then be added together to form a lattice which preserves the electromagnetic properties

MM \ Sub		n=1			n=2			n=3	
									
	pm	pmm	p4m	cm	cmm	p4m	p2	pg	





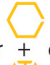


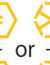

MM \ Sub		n=1			n=2			n=3	
									
	p6m	pmm	cm	pm	pmm	cm	p3m1	p1	

Fig. 1. Group classification for two dimensional metamaterial designs.

of each sub-lattice. In our particular study we investigate planar geometries and thus consider various wallpaper groups [19]. For example, if we are interested in constructing a material with two distinct elements (bipartite), then a planar MM array can be generated in a straightforward manner, e.g. a checkerboard pattern. This has already been achieved in efforts to eliminate bianisotropy in planar SRR arrays [20] and to create dual resonance behavior [22]. However this arrangement may be less desirable when moving to three elements (tripartite) or more. This is due to the fact that the most effective geometry is one that will allow for maximum filling fraction in order to maximize the EM response, i.e. oscillator strength [8]. Thus we should appeal to unit cell symmetries different than square if we are interested in achieving metamaterials with three or more distinct elements. Considering only two-dimensional designs there are limited primitive cell choices, and only parallelogram, triangular, and hexagonal shapes can tile the whole surface - utilizing translation, reflection, and rotational symmetries - without leaving gaps in-between. Most metamaterial designs to-date use square lattices - a special case of parallelogram[21].

Fig. 1 shows the group classification for two dimensional metamaterial designs using either square or hexagonal unit cells. Appealing to the formalism of two dimensional wallpaper groups, the top portion of Fig. 1 gives all the possible groups resulting from the combination of square primitive cells up to n=3 with different structures. For example, by placing one of the three square MMs together (under the n=1 heading) and tiling the entire surface, the pattern belongs to the group *pm*, *pmm* or *p4m*. Columns under the n=2 heading show groups with two different MMs in one unit cell. In this case the MMs may tile the surface as a checkerboard pattern. The last n=3 columns give groups that are combinations of three primitive cells spanned by two tiling vectors are along -30 and 30 degrees. We consider the case that if there is more than one primitive cell per structure, that MMs with the same symmetry are distinct, i.e. they are resonant at different frequencies.

The bottom part of Fig. 1 shows groups that correspond to hexagonal primitive cells and MMs. A single hexagon shape and its tiling to the entire two dimensional surface belongs to the group *p6m*. This group is of highest symmetry among all the 17 wallpaper groups, and has rotations of order $s = 2, 3$ and 6, (where we define a rotation as $2\pi/s$ radians), as well as various reflection symmetries. Adding any lower symmetry object to the hexagon will reduce

the symmetry, as detailed under the $n=1$ heading. If the number of hexagons in one primitive cell continues to increase, the symmetry of the two dimensional pattern will keep decreasing. For unit cells composed of $n=2$ MMs, the tiling vectors are along 0 and 60 degrees. Unit cells consisting of $n=3$ MMs, (with the three primitive cells being nearest neighbors), the tiling vectors are along 0 and 60 degrees. Here, as with square unit cells, we consider hexagonal MMs with the same symmetry to consist of unique designs. When the number $n \geq 5$ there will be no rotational or reflection symmetry at all, belonging to group $p1$, which is the group with the lowest symmetry in two dimensional wallpaper groups.

For a given design consisting of one primitive cell, the filling fraction depends on the ratio of the area enclosed by metamaterial to the area of the unit cell [8]. The frequency dependence of the metamaterial response functions is given as:

$$\tilde{\epsilon}(\omega), \tilde{\mu}(\omega) = \epsilon_{\infty}, \mu_{\infty} + \sum_m \frac{F_m \omega^2}{\omega_{0m}^2 - \omega^2 - i\Gamma_m \omega} \quad (1)$$

where ω_0 is the center frequency of the m^{th} oscillator, $\mu_{\infty}, \epsilon_{\infty}$ are the real parts of μ, ϵ at $\omega = \infty$, and Γ is the loss. The term F_m is the filling fraction of the m^{th} oscillator and is given as,

$$F_m = \frac{a_m}{nA} \quad (2)$$

where a_m is the area of the m^{th} metamaterial element, n is the total number of distinct primitive cells, and A is the area of the primitive cell. The exotic behavior of metamaterials, e.g. negative refraction, is obtained by maximizing the element response such that negative parameters are obtained. As such it is important to make the unit cell and the metamaterial element the same shape, i.e. both square, or both hexagonal, in order to maximize the filling fraction, and thus the electromagnetic response. Increasing the number of primitive cells with different elements will sharply decrease F_m , roughly dividing by the number of primitive cells in a given design, as shown in Eq. 2.

3. Simulation

In order to determine the correct dimensions and geometry for resonant THz metamaterials consisting of multi-unit cells, we simulated various structures of similar size to previous work [23]. Metamaterials were computationally designed using a commercial simulation package HFSS from Ansoft [24]. As a general starting point for our structures an electric metamaterial was chosen due to its strong interaction with a normally incident electromagnetic wave [11]. For metamaterials consisting of $n=2$ square unit cells (e.g. Fig. 4 (e)) we use simple Perfect Electric Conductor (PEC) and Perfect Magnetic Conductor (PMC) boundary conditions on the lateral faces of the unit cell. Waveguide ports on the other boundaries then approximate propagation of a plane wave incident on the metamaterial structure.

For structures consisting of $n=3$ or more different primitive cells, we utilize a more amenable geometry ideal for maximization of the electromagnetic response, as determined by Eq. 2. As such we use an underlying hexagonal unit cell, where the electric metamaterials are then modified to maximize the filling fraction, as shown in Fig. 4(a)-(d). Obviously for this type of unit cell, the conventional boundary conditions described above are unsuitable, and thus we use Periodic Boundary Conditions (PBCs). A local coordinate system is created on each surface and the field of one surface is mapped onto another. Assignment of these boundary conditions is done by grouping the outer surfaces of the model into pairs. For example, Fig. 2(a) shows the unit cell for a $n=3$ metamaterial. Numbers around the perimeter denote a particular surface and each is mapped to its pair. In this way we are able to simulate a metamaterial infinite in extent in the lateral directions. Plane wave ports on the front and back faces then permit frequency

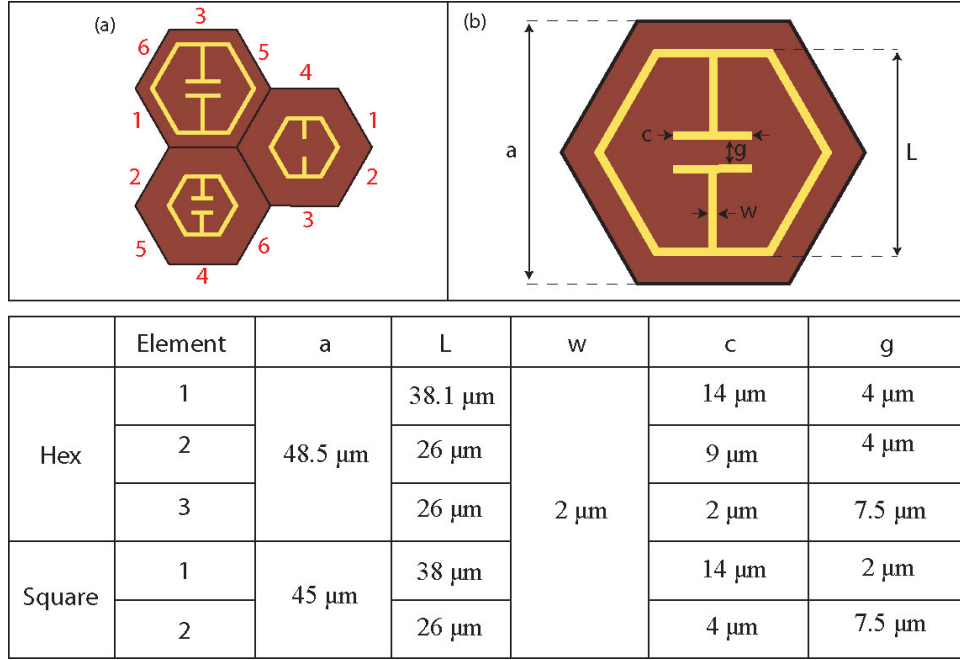


Fig. 2. Simulated unit cell and a single primitive cell. (a) Diagram of simulated $n=3$ hexagonal MM. Also shown are the assigned periodic boundary pairs used in simulation. (b) Single primitive cell with dimensions labeled. The lower portion of the figure gives the values of the labeled parameters used in our designs.

dependent computational studies of the complex S-parameters, i.e. transmission ($T=|S_{21}|^2$) and reflection ($R=|S_{11}|^2$). Similar boundary mappings are used for the $n=1$ metamaterial structures shown in Fig. 4 (a)-(c).

Simulated electric fields and current densities for the $n=3$ hexagonal metamaterials are shown in Fig. 3(a)-(c). We have designed a metamaterial with three separate distinct structures, and as such, we expect each sub-lattice of the metamaterial to be resonant at different frequencies. Computational results shown in Fig. 3 (a)-(c) verify that this is the case. For example, at $\omega_1 \equiv 0.53$ THz the metamaterial element in the top left of the unit cell is resonant, as verified by the enhanced electric field located within the gap, as well as the significant current density - denoted by the red cones. The other two elements resonate at $\omega_2 \equiv 0.99$ THz and $\omega_3 \equiv 1.26$ THz respectively. The electric field is plotted over the entire unit cell, while current density only on the surface of each metamaterial. These two parameters are normally out of phase by 90 degrees, the current densities shown in Fig. 3 have been shifted to highlight the resonant response. This verifies that at each of the frequencies ω_1 , ω_2 , and ω_3 only a single element is active, meaning that the combined metamaterial will behave as if it was a single element structure over a frequency range.

We now turn to the simulated transmission obtained for the various metamaterial structures shown as the black curves in Fig. 4. Each of the $n=1$ hexagonal metamaterials, shown in Fig. 4 (a)-(c) yield transmission minima at $\omega=0.53$ THz, $\omega=0.99$ THz, and $\omega=1.26$ THz, respectively. Away from resonance values of $T = 60-70$ percent are achieved, and minima at resonance are below 10%. Each of the unit cells shown in Fig. 4 (a)-(c) are used as primitive cells and combined into a $n=3$ structure, as depicted in Fig. 4(d). Each of the independent resonances

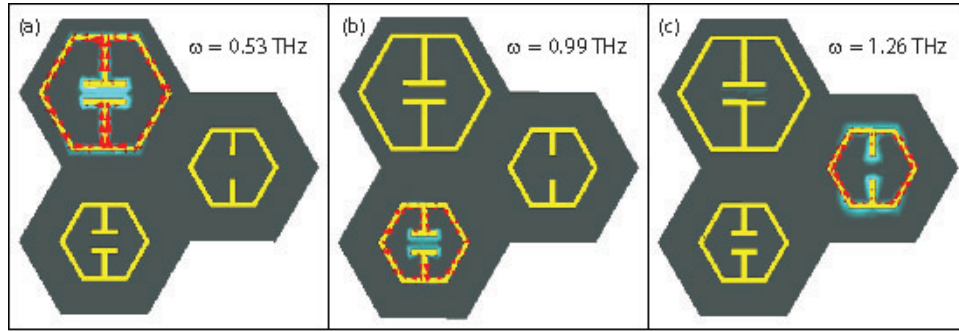


Fig. 3. Simulated electric field and surface current for $n=3$ hexagonal metamaterial (a) current density and electric field plots at ω_1 (b) current density and electric field plots at ω_2 (c) current density and electric field plots at ω_3

are preserved in this combined metamaterial structure, and we observe resonance at $\omega=0.53$ THz, $\omega=0.99$ THz, and $\omega=1.32$ THz. As a verification of the versatility and engineerability of metamaterials, we also design a $n=2$ square checkerboard structure which also yields the same three resonant frequencies, i.e. ω_1 , ω_2 , and ω_3 , shown in Fig. 4 (e). In this case for the highest frequency resonance, we utilize the cut-wire response of the metamaterial, rather than a distinct element[25].

4. Fabrication

The metamaterials were fabricated at Boston University utilizing a standard lift off process. AZ5214e image reversal photoresist was spin-coated on HMDS-coated SI-GaAs wafer at 4,000rpm for 40s yielding a thickness of $1.5 \mu\text{m}$ and baked on the hot plate at the temperature of 110°C . The photoresist was exposed to UV light to pattern the metamaterial structures. A 150s hard bake was performed on a 120°C hot plate, followed by flood-exposure for 60s. The wafer was then developed in the AZ 400K (1:4 diluted) for 15s to dissolve the resist where the metal should be deposited and rinsed in the DI water for 60s. A 10nm Ti layer was first deposited to improve the Au layer adhesion, and then a 200 nm-thick Au layer was evaporated using Sharon E-beam evaporator and then lifted off by rinsing in acetone for several minutes. Various images of the fabricated metamaterials are shown in Fig. 4.

5. Experiment

All metamaterial samples were characterized at Boston College using a Fourier Transform Infrared (FTIR) spectrometer. THz radiation from a mercury arc-lamp, was polarized before impinging on MM samples at normal incidence. The transmitted THz was then refocused on a liquid helium silicon bolometer and recorded as a function of mirror step position of the FTIR. Etalons due to multiple reflections within the GaAs substrate were removed and the modified interferogram was Fourier transformed to obtain the sample spectrum. A similar procedure was performed for a reference with an open channel and division of the sample and reference spectra resulted in the frequency dependent absolute value transmission $T(\omega)$.

In the right column of Fig. 4 we show experimental transmission (red curves) of the metamaterials. Each metamaterial sample yields a resonant response in the THz frequency range. For example, the sample shown in Fig. 4(a) yields low frequency transmission values near 50 percent before a minimum occurs, yielding a value of 12 percent at 0.5 THz, before recovering

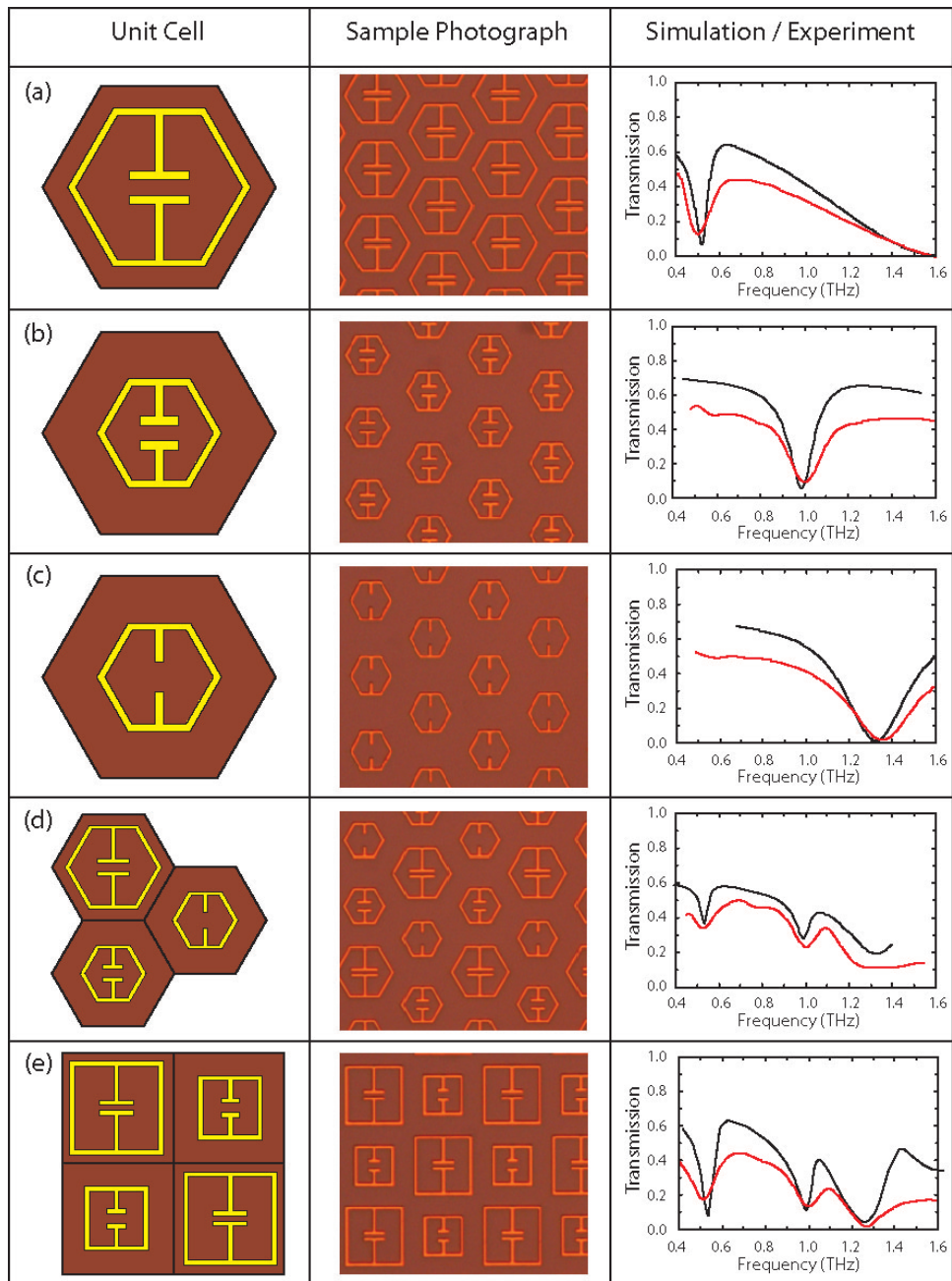


Fig. 4. Simulation and experimental results for our different $n=1,2$, and 3 metamaterial designs. The left column shows the unit cell models, images taken of the fabricated samples are in the middle column, and plots of simulated (black curve) and experimental data (red curve) are shown in the right column.

back to relatively high values. At higher frequencies, the curve tends toward $T=0$, as higher order resonances occur. Similar behavior is observed for the other $n=1$ hexagonal metamaterial elements, with resonances at $\omega=1.0$ THz (Fig. 4(b)), and $\omega=1.35$ THz (Fig. 4(c)). When all of the three individual metamaterial elements are combined into a single structure (Fig. 4(d)), resonances observed in the individual hexagonal metamaterials are preserved with very little change in frequency location.

Electromagnetic responses to that of the $n=3$ hexagonal structure, can be designed and obtained for a $n=2$ square metamaterial. In Fig. 4(e) the red curves show $T(\omega)$ for the square $n=2$ checkerboard metamaterial. Transmission minima occur at $\omega=0.51$ THz, $\omega=1.0$ THz, and $\omega=1.26$ THz, in great agreement with that obtained for the $n=3$ hexagonal MM. Notice in this case, that although transmission maxima are similar, i.e. $T\sim 40\text{-}50\%$, that oscillator strengths are greater for the square $n=2$ lattice compared to that of the $n=3$ hexagonal metamaterial. In the former, minima in $T(\omega)$ are all 20% or lower, whereas in the latter they range between 20 and 40%. This can be understood directly from Eq. 2, since the oscillator strength F_m is inversely proportional to the number of elements (n).

6. Discussion

We now turn toward highlighting some potential applications of these planar wallpaper group metamaterials. The frequencies of roughly $\omega=0.5$, 1, 1.25 THz have been specifically chosen in order to investigate the possibility of metamaterials to act as bio-detectors, or as a means of electromagnetic mimicry. For example, the resonant frequencies of our metamaterials were designed to coincide with the electromagnetic resonances of the molecule biotin, ($C_{10}H_{16}N_2O_3S$) also known as vitamin H or B₇. These natural resonances result from rotational, twisting, or vibrational modes and typically occur in the microwave through THz and far infrared ranges of the electromagnetic spectrum [31, 32]. As such, biotin is an excellent molecule to benchmark possible bio-detection methods at THz frequencies. The grey curves of Fig. 5 show the measured THz transmission spectra of biotin, (powdered form), which reveal three resonances at $\omega=0.5$ THz, $\omega=1.0$ THz, and $\omega=1.26$ THz, consistent with previous data [31].

Most proposed ideas for bio-detection utilizing metamaterials involve using the enhanced electric fields near or within the gap of split-rings [33, 34]. In this scheme, when the desired particle comes into the vicinity of the gap there is a change in the resonant frequency (ω_0) of the metamaterial, due to the sensitivity on the capacitance (C), i.e. $\omega_0 \sim 1/\sqrt{C}$. In-fact the discovery publication [8] on split-ring resonators highlighted the enhanced field within the gap and suggested its use as a means to enhance non-linear phenomena. Indeed experimental results at THz frequencies have verified the extent to which features of the metamaterial resonance can be controlled by varying gap properties [29, 30]. However it should be mentioned that the above methods [33, 34] are prone to contaminants which may cause false positives in identification. For example, *any dielectric which lies in vicinity of the gap* has the ability to modify the resonant frequency. Thus particles as common as - say - dust and pollen will be severely problematic.

However, it may be possible to perform bio / chemical detection with metamaterials by non-linear processes in analogy with surface enhanced Raman scattering (SERS), or more closely, surface enhanced infrared absorption spectroscopy (SEIRA) [35]. This idea is based on the significant field enhancement which occurs within the gaps of SRRs. Simulations indicate that within the gaps of the metamaterial the on-resonance electric field for the structures shown in Fig. 3 is of order $10^6 - 10^7 \text{ V}\cdot\text{m}^{-1}$ when illuminated with a power of $10^4 \text{ W}\cdot\text{cm}^{-2}$. Knowing the specific resonance frequencies of a particular substance is the first step for building such a device. Identification of a molecular hazard could then be achieved by examining how the metamaterial and molecule, which are both resonant at the same frequency, behave upon binding of

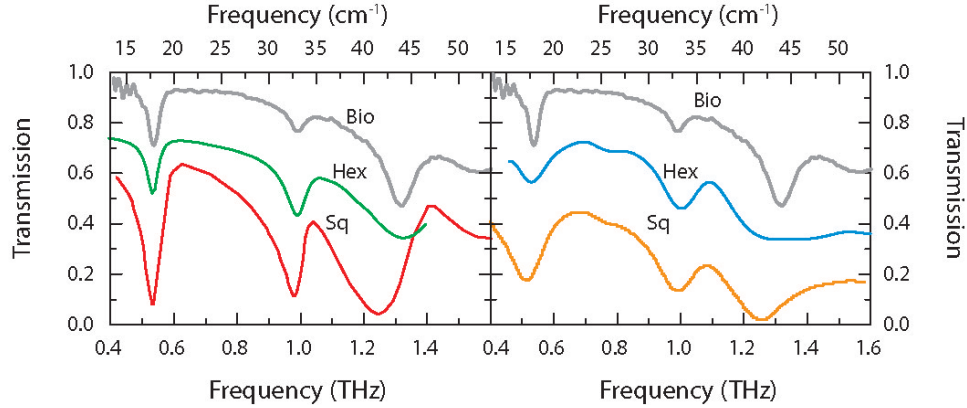


Fig. 5. Computational (left) and experimental (right) measurements of the $n=3$ hexagonal metamaterial, and the $n=2$ square checkerboard metamaterial, compared to experimental measurements of the molecule biotin. Simulated and experimental transmission spectra of the hexagonal metamaterial has been shifted up by 20% for clarity and $T(\omega)$ of biotin is in arbitrary units.

the molecule within the SRR gap. The response of the SRR array (with biotin occupying the gap) will yield an enormous, perhaps non-linear response, thus increasing the sensitivity by as much as 10^6 - typical with driven resonances or overlapping resonant phenomena [36, 37]. In addition, previous work has shown that the THz resonances of biotin have anharmonicity constants ranging from 10^{-4} to 10^{-3} [31]. Thus another possible identification method involves detection of the sub or super-harmonic modes created upon excitation. In short, nonlinearities associated with overlapping resonant metamaterials and molecular responses, through engineering metamaterials to a bio or chemical hazard of interest, will provide an interesting approach beyond simple dielectric induced resonance shifts.

In order to negate false positives, proper identification of a material may require more than a single frequency match. As demonstrated throughout this paper a salient feature of metamaterials is the ability to create a structure that yields resonances at several frequencies. This scheme, often called “fingerprinting” would then utilize several points of comparison to ensure accuracy. An initial study has been carried out and in Fig. 5 we show a comparison of $T(\omega)$ of biotin to various metamaterial structures. Both the $n=2$ square MM and the $n=3$ hexagonal MM, achieve a good match to biotin, right panels. Thus when biotin lies in proximity to various gaps of the structure, the MM resonances (when excited by THz radiation) will overlap with the THz resonances of biotin. Future detection could be enhanced by patterning specific binding agents to metamaterial gaps. In the case of biotin the protein avidin could be used, which has an affinity of order 10^{15} M^{-1} . [38] Whatever the desired molecule or agent of interest, site specific binding can yield reductions in false positives, and may help to increase the sensitivity of detection.

Another potential application of metamaterials demonstrated here is that of electromagnetic signature control. For example - from the viewpoint of interrogating THz radiation - both our $n=2$ square and $n=3$ metamaterials look nearly identical to biotin. Thus utilizing the methods shown here for the design and fabrication of metamaterials, one could construct materials, or the surfaces of structures, to mimic another substance. Further, recently it has been shown possible to fashion metamaterials as perfect absorbers, both at microwave [39] and THz [26]. Kirchhoff’s law of thermal radiation dictates that the emission spectra of such a metamaterial

should then be, at thermal equilibrium, equal to that of the absorption spectrum. Thus, with multi-unit cell ideas here, combined with perfect absorber techniques, one can design a specific emission spectra for an object at a given temperature, i.e. engineer its blackbody spectra.

7. Conclusion

Our results verify that multiple element metamaterials can be successfully designed, fabricated, and measured at THz frequencies. Two different structures were used to obtain resonances at roughly $\omega=0.5$ THz, $\omega=1$ THz, and $\omega=1.25$ THz. We have constructed a metamaterial structure composed of three hexagonal sub-elements that mimic the resonant behavior seen in the molecule biotin. The simulated and the experimentally measured transmission were also in good agreement. Hexagonal structures opens up potential new methods for creating multiple resonator metamaterials. Such multi-resonator metamaterials may provide a quick method for fingerprinting and detection of chemical and biological agents based on nonlinearities associated with the electric field enhancement within the capacitive gaps, or as materials to facilitate electromagnetic signature control.

Acknowledgement

WJP and CMB acknowledge support from the Office of Naval Research (ONR), grant N000140710819. RDA and XZ acknowledge support from NSF EECS 0802036. The authors would also like to thank the Photonics Center at Boston University for technical support.